Emergence of Localized States in Narrow GaAs/AlGaAs Nanowire Quantum Well Tubes

ARTICLE *in* NANO LETTERS · FEBRUARY 2015

Impact Factor: 13.59 · DOI: 10.1021/nl5046878 · Source: PubMed

NANO LETTERS

Letter

pubs.acs.org/NanoLett

Emergence of Localized States in Narrow GaAs/AlGaAs Nanowire Quantum Well Tubes

Teng Shi, Howard E. Jackson, and Leigh M. Smith*

Department of Physics, University of Cincinnati, Cincinnati, Ohio 45221-0011, United States

Nian Jiang, Qiang Gao, H. Hoe Tan, and Chennupati Jagadish

Department of Electronic Materials Engineering, Research School of Physics and Engineering, The Australian National University, Canberra, ACT 0200, Australia

Changlin Zheng and Joanne Etheridge

Monash Centre for Electron Microscopy, Monash University, Victoria 3800, Australia

Supporting Information

ABSTRACT: We use low-temperature photoluminescence, photoluminescence excitation, and photoluminescence imaging spectroscopy to explore the optical and electronic properties of GaAs/AlGaAs quantum well tube (QWT) heterostructured nanowires (NWs). We find that GaAs QWTs with widths >5 nm have electronic states which are delocalized and continuous along the length of the NW. As the NW QWT width decreases from 5 to 1.5 nm, only a single electron state is bound to the well, and no optical excitations to a confined excited state are present. Simultaneously, narrow emission lines (fwhm < 600 μeV) appear which are localized to single spatial points along the length of the NW. We find that these quantum-dot-like states broaden at higher temperatures and quench at temperatures above 80 K. The lifetimes of these localized states are observed to vary from dot to dot from 160 to 400 ps. The presence of delocalized states and then localized states as the QWTs become more confined suggests both opportunities and challenges for possible incorporation into quantum-confined device structures.

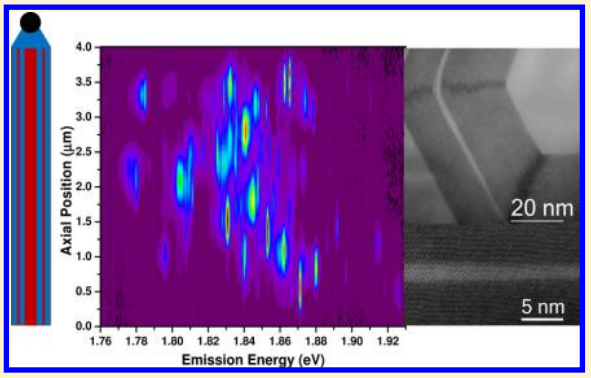

KEYWORDS: *Nanowires, heterostructures, quantum well, excitation spectroscopy*

Semiconductor nanowires (NWs) are excellent candidates for development of novel nanodevices such as solar cells, thermoelectrics, water splitting, single-photon emitters, light-emitting diodes, and lasers.[1−9] They also are the basis for novel materials for fundamental science such as Majorana fermions and topological insulators.[10] Presently there is particularly intense interest in pushing the NWs to smaller dimensions where electronic states could be strongly confined perpendicular to the NW axis yet free to move along the axis. Achieving the strong confinement limit is particularly challenging because of both the extreme sensitivity of growth to surfaces and the challenge of passivation of the surface in such small-diameter wires. The ability to control the geometry of the NW should open a wide range of new science, new technologies, and applications.

In light of this, rapid developments have appeared in the past 2 years toward using core−multishell structures to create novel heterostructures where two-dimensional (2D),[11] one-dimensional (1D),[12−15] and zero-dimensional (0D)[16,17] electronic states can be created in the strong confinement limit and which utilize the unique symmetries determined by the growth crystal axis. Such states have the advantage that they are buried within the shells surrounding the NW and so are isolated from free surfaces. Thus, effects such as nonradiative recombination and Fermi-level pinning are mitigated. A number of investigations have reported 0D quantum dots (QDs) which are formed within an AlGaAs barrier surrounding the GaAs core through either alloy fluctuations or unusual physical structures at the corners of 111-grown wires.[16,17] In addition, 0D QDs formed by Stranski−Krastinow-like strained growths at or along the facets of the NW have been reported.[18] Here we consider electron and hole states which are confined to uniform GaAs quantum wells which are wrapped around the central hexagonally symmetric GaAs core and which are embedded within the AlGaAs barrier material.

Received: December 6, 2014
Revised: February 16, 2015
Published: February 25, 2015

DOI: 10.1021/nl5046878
Nano Lett. 2015, 15, 1876−1882

Several theoretical calculations have shown that the ground states of this system are localized to the corners of the quantum well which is wrapped around the hexagonal facets and which effectively forms 1D quantum wires which run along the length of the NW.[12−15] Photoluminescence (PL) and photoluminescence excitation (PLE) measurements in GaAs/AlGaAs quantum well tubes (QWTs) have shown that the confined states are consistent with these calculations.[12] Initial experimental results on modulation-doped wires have been promising.[11,15] Even in modulation-doped simple core−shell GaAs/AlGaAs NWs, both electrons and holes can form 1D wires in certain circumstances.[11,13,15] Theoretical calculations of these unusual quantum states in magnetic fields show a mixture of Aharonov−Bohm-like behavior along with Landau levels, depending on the orientation of the magnetic field relative to the NW.[13,14] In this Letter, we report on spatially-resolved experiments on QWTs for well widths which range from 8 down to 1.5 nm, and show that there is a transition from delocalized 1D-like states for the wider wells to 0D-like electronic states for narrower wells. The 0D-like states likely result from well-width or alloy fluctuations, similar to what is seen in epitaxial 2D GaAs/AlGaAs quantum wells.

Nanowire Growth and Structural Characterization. In this work, a series of GaAs/AlGaAs QWT NWs with different QWT widths were grown by metalorganic chemical vapor deposition to address the impact of the QW thicknesses. Trimethylgallium (TMGa), trimethylaluminum (TMAl), and arsine (AsH_3) were used for the source of Ga, Al, and As, respectively. First, GaAs NWs were grown on GaAs (111)B substrates by a two-temperature procedure using Au nanoparticles with a diameter of 50 nm as the catalysts.[19] After the NW core growth, the growth temperature was increased to 750 °C and then a 23 nm AlGaAs layer was deposited surrounding the core, followed by the GaAs QWT growth by switching off TMAl. The thicknesses of GaAs QWT, nominally ranging from 1.5 to 8 nm, were controlled by the growth time. The GaAs QWT was then enclosed in another AlGaAs layer with the thickness of 12 nm. As a result, a GaAs QWT sandwiched between two AlGaAs layers was obtained in the NW. Finally, a thin layer of GaAs was deposited as a capping layer to prevent the oxidation of Al in the AlGaAs shell.

The QWT cross-sectional structures are characterized by aberration-corrected high-angle annular dark field scanning transmission electron microscopy (HAADF-STEM) using a FEI Titan^3 80-300 Schottky field emission gun TEM/STEM fitted with spherical aberration-correctors (CEOS GmbH) on the probe and image forming lenses and operating at 300 kV. Figure 1a shows an overview of the cross-sectional morphology of a 1.5 nm QWT NW. In this atomic-number sensitive imaging mode, the QWT appears as a concentric light band (indicated by the red arrow) embedded in the darker AlGaAs buffer layer. As observed previously, the morphology shows a 3-fold symmetry around the growth axis associated with the crystal structure polarity.[20] Figure 1b−d shows atomic resolution images of a section of the 1.5, 2, and 6 nm QWTs, respectively, which lie parallel to the {110} planes. The experimental parameters were characterized quantitatively[21] so that the aluminum composition in the AlGaAs layers can be determined from the HAADF-STEM image intensity.[22] The color encoded aluminum composition map from a 1.5 nm QWT sample is shown in Figure 1e (the composition is represented by the color bar on the right) along with the atomic resolution image shown above. The average aluminum concentration in the AlGaAs buffer layer is measured from this image to be 0.40 ± 0.06. Additional HAADF-STEM images of the complete set of QWT NWs considered here can be found in the Supporting Information

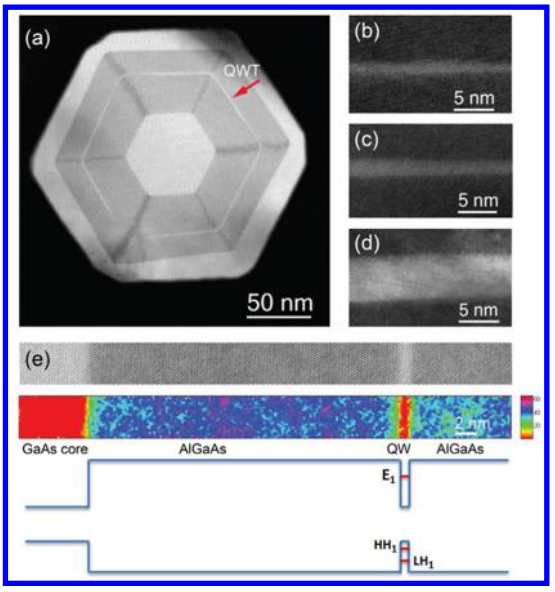

Figure 1. HAADF-STEM images of QWT NW cross sections. (a) Low-magnification overview of a 1.5 nm QWT NW. (b−d) Atomic resolution HAADF-STEM images of the 1.5, 2, and 6 nm QWTs, respectively. (e) Atomic resolution image of a 1.5 nm QWT and associated map of the aluminum concentration in the AlGaAs buffer layer determined from a quantitative analysis of the HAADF-STEM image. Schematic of valence and conduction band alignments on same scale as images.

Single Nanowire Optical Characterization Including PL, PLE, and TRPL. We use PL, PLE, time-resolved PL, and spatially resolved PL map measurements of single NWs in order to explore the optical and electronic properties of this series of QWTs. The QWT NWs were dispersed onto clean marked silicon substrates, mounted onto the copper coldfinger of a liquid helium constant flow cryostat, and then cooled to 10 K. Tunable excitation was provided by a 800 nm, 76 MHz pulsed Ti-sapphire laser which pumps a photonic crystal fiber to create a white light continuum from 500 to 1200 nm. Using a prism filter, a narrow 3 nm wide band for excitation can be selected and scanned over this wavelength range. The pulsed excitation was focused through a 50×/0.5NA microscope objective onto a single NW. The PL emission was collected through the same objective, imaged onto the entrance slit of a spectrometer, dispersed by a grating, and then detected by a cooled charge-coupled device (CCD).

Low-temperature PL and PLE measurements for single 1.5, 2, 3.5, and 6 nm QWTs are displayed in Figure 2. PL is shown as solid lines; these QWT NWs have high quantum efficiency with a dominant emission from the QWT with excitation powers in the sub-microwatt range as previously observed.[12] Red solid lines centered at 1.515 eV represent the emission from the GaAs core state, corresponding to the typical zincblende GaAs free exciton emission.[23−25] The line widths of the core emission varies slightly from wire to wire and may reveal differences in the GaAs core quality. More interesting are emissions from the QWT n = 1 electron and hole ground states, represented by the black solid lines. The strong effects of quantum confinement in these NWs are displayed by the

DOI: 10.1021/nl5046878
Nano Lett. 2015, 15, 1876−1882

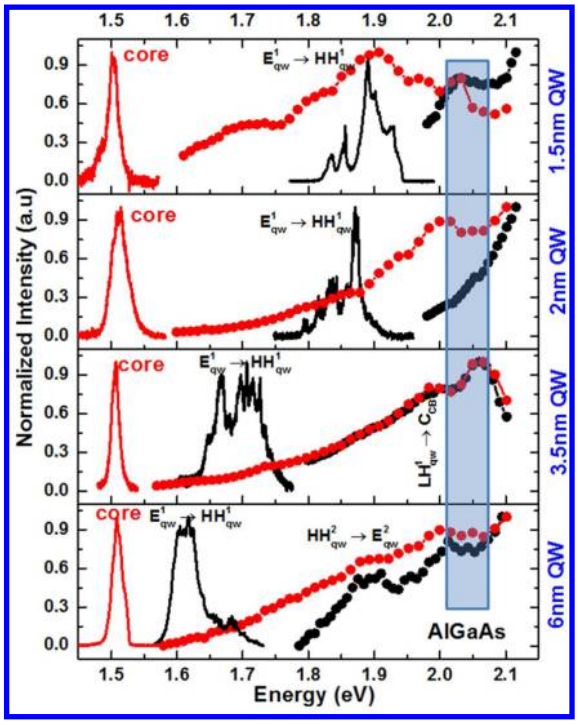

Figure 2. Low-temperature photoluminescence and photoluminescence excitation measurements for single 1.5, 2, 3.5, and 6 nm QWT NWs. PL and corresponding PLE spectra associated with the GaAs core are shown in red solid lines and symbols; PL and corresponding PLE spectra associated with the QWT emission are represented by black solid lines and symbols. Maximum intensities of all spectra are normalized to unity.

upward shift of emission energies from 100 meV (6 nm QWTs) to 400 meV (1.5 nm QWTs) above the core GaAs band edge emission. As the confinement energy increases with smaller well width, the full width at half-maximum (fwhm) of the emission band also increases about 30 meV. One begins to observe very narrow QD-like emissions for QWTs with widths less than 5 nm. Note that emission from the AlGaAs barriers could not be seen in any of the PL spectra, which is consistent with extremely efficient capture of carriers into the QWTs.

PLE spectra associated with the GaAs core (red dots) and QWT (black dots) emission were taken under the same excitation conditions. PLE spectra were obtained by integration of the core and QWT emissions at each wavelength to create the excitation spectra shown by the red and black symbols at higher energy. Both the core and QWT emissions show strong excitations (pale blue bar, Figure 2) associated with the AlGaAs continuum, indicating an aluminum concentration between 0.4 and 0.45, consistent with the TEM results discussed earlier. The PLE associated with the GaAs core (red dots) for the 2, 3.5, and 6 nm QWTs exhibit *only* the excitation peak associated with the AlGaAs barrier. When the laser is scanned through the QWT ground state, there is no associated peak in the PLE spectrum which indicates that the QWT states are well isolated and not coupled to the GaAs core. Interestingly, the $n = 2$ hole-to-electron transition for the 6 nm QWT as well as the $n = 1$ transition for the 1.5 nm QWT are observed in the core PLE spectra for these NWs, indicating that these states which are only a little below the AlGaAs continuum are coupled to the core.

Similar to the core PLE spectra, the PLE spectra associated with QWT ground state emission all show excitation peaks associated with the AlGaAs barrier. In addition, the 6 nm QWT shows a prominent peak associated with absorption from the $n = 2$ heavy hole-to-electron states. For narrower QWTs, however, there is only one bound state for electrons, and so only bound electron or hole to the AlGaAs continuum excitations are observed.

Model for Quantum Well Tubes in Nanowires. To interpret the spectral features observed in these PL and PLE measurements, we have calculated the quantum-confined states in the QWT NWs. Based on the structural information obtained from the HAADF-STEM cross-sectional images, we carried out an eigenfunction expansion method to calculate the confined energy levels for both electrons and holes.[12] A simplified cylindrically symmetric model has been considered with a 25 nm radius GaAs core, a 23 nm-thick AlGaAs shell, a GaAs QW with thickness ranging from 1 to 10 nm, followed by an outer 22 nm AlGaAs layer. We use the eigenfunction expansion method using 100 zero orbital angular momentum basis wave functions within a finite QWT potential to calculate the quantum-confined energies and wave functions for electrons (E), heavy holes (HH), and light holes (LH). This method has been discussed in detail by Fickenscher et al.[12]

Using these simulations of the quantum-confined electron and hole states we can calculate the energies of the optical transitions between the $n = 1$ and $n = 2$ electron- and the hole-confined states. The results of these calculations as a function of QWT width for 40% (blue solid squares) and 45% (red solid line) AlGaAs barriers are shown in Figure 3. The widths of the

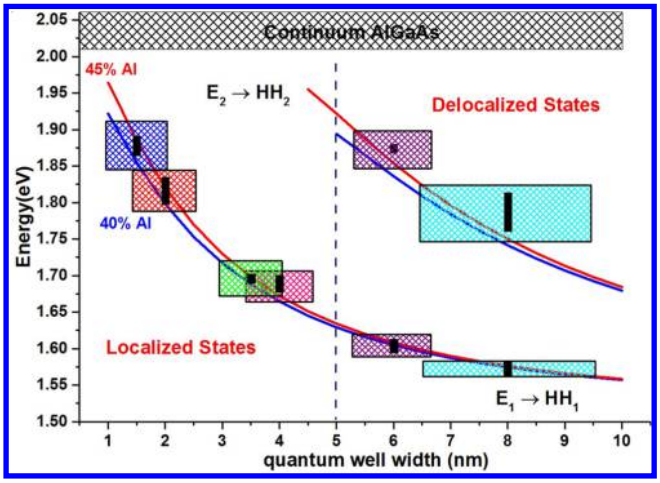

Figure 3. Cylindrically symmetric eigenfunction expansion calculations show numerical results for $n = 1$ and $n = 2$ states for QWTs with different well widths and Al concentrations. Colored boxes indicate the experimentally observed well-width fluctuations and fwhm of the GaAs QWTs as widths and heights, respectively. Black bars represent the maximum and minimum energy centers of the PL or PLE peaks taken from multiple NWs.

colored shaded boxes indicate fluctuations of the QWT widths extracted from the high resolution cross-sectional images, while the heights represent the fwhm obtained from the PL spectra of the 1.5 (blue), 2 (red), 3.5 (green), 4 (pink), 6 (purple), and 8 nm (cyan) QWT NWs. (The values for the 4 and 8 nm QWT energies are taken from ref 12.) The black bars show the range of energies observed for multiple NWs, the center of the boxes show the average of these NWs. While the thinner wells are certainly disordered, the variation in emission energy is less than the line width in every case.

DOI: 10.1021/nl5046878
Nano Lett. 2015, 15, 1876−1882

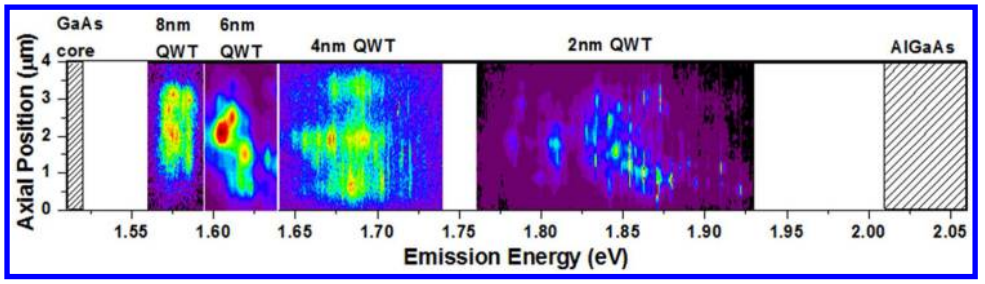

Figure 4. Two-dimensional PL maps vs distance along the nanowire from single 8, 6, 4, and 2 nm QWT NWs at 10 K under nonresonant excitation. Shaded areas represent the GaAs cores (1.515 eV) and the AlGaAs barriers (2.01 eV).

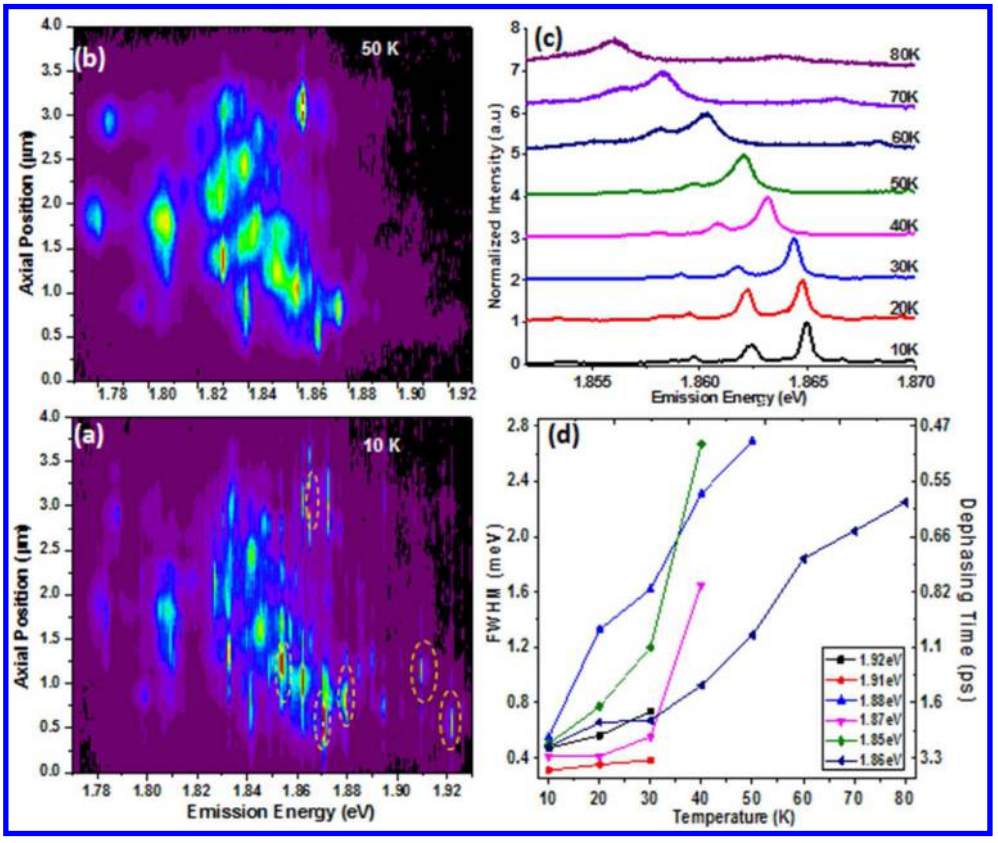

Figure 5. PL images at (a) 10 and (b) 50 K, showing that the localized states quench at higher temperatures. The evolution of single peaks with temperature, with the line width reflecting dephasing times, is shown in (c) and (d) for selected localized states.

The numerical results show that only a single electron-confined state exists in QWT NWs with well widths smaller than 5 nm, so that no $n = 2$ excitation (HH2 → E2) should exist for such QWTs. When the QWT well widths become larger than 5 nm, transitions from electron and hole excited states begin to appear. We have identified $n = 2$ (HH2 → E2) optical transitions in the 8 nm QWT[12] as well as the 6 nm QWT, both shown in the data in Figure 3.

Photoluminescence Spatial Imaging of Localized States. Single NW PL spectra for QWTs with well widths smaller than 5 nm show the presence of very sharp peaks. In contrast, sharp lines are not observed on any QWT NWs with well widths larger than 5 nm. The sub-meV line widths of these sharp emission spectra are consistent with the localization of excitons within the QWTs. To confirm this localization, single NW imaging using slit confocal microscopy was implemented using a high index glass hemisphere which is mounted using an indium ring to the coldfinger of a cryostat.[26−28] QWT NWs were transferred onto the geometric center of a 4 mm hemispherical solid immersion lens (SIL, with a refractive index $n = 2$), and NWs were oriented with the image of the long axis lying parallel to the entrance slit of the spectrometer. A defocusing lens was used to expand the excitation laser so that the NW was uniformly illuminated and the PL emitted from the NW was imaged onto the entrance slit of the spectrometer. After being dispersed by the grating, the PL image was detected by a 1024 × 124 pixel Si CCD so that the vertical (short) axis provided spatial resolution while the horizontal (long) axis of the CCD provided energy resolution. Using the SIL substantially increased the spatial resolution to ∼500 nm, and the collection efficiency simultaneously increased substantially.[26−28]

Figure 4 shows false-colored 2D PL maps obtained from four different QWT NWs with well widths ranging from 8 to 2 nm at 10 K. The vertical axis of the map indicates the spatial location of the PL emitted from single QWT NWs of 4 μm length, while the horizontal axis represents the emission energy. The diffraction limited optical resolution of the image is 500

DOI: 10.1021/nl5046878
Nano Lett. 2015, 15, 1876−1882

nm. The energies associated with the GaAs core and AlGaAs barrier are noted by the striped vertical bars in the figure.

As the QWT well width decreases from 8 to 2 nm, the emission energy rapidly increases reflecting the increasing quantum confinement of the excitons. The 8 and 6 nm QWT maps show PL emission which is approximately continuous along the NW axis. In contrast, PL images from the 4 and 2 nm QWT NW show many ultranarrow emission lines which are emitted from a single spatial location along the NW axis. As the well width decreases, the average range of emission energies increases substantially from 20 meV in the 8 nm QWT to 140 meV in the 2 nm QWT. This increased line width may reflect increased roughness of the QWT, but also reflects the sensitivity of the emission energy to well-width fluctuations or concentration fluctuations in the AlGaAs barriers for small well widths.

Several reports in GaAs/AlGaAs QWT structures which show strong QD-like sharp emissions have been interpreted as coming from within the AlGaAs barriers either from specific regions near the corners of the QWT,[16] or from alloy fluctuations within the AlGaAs itself.[17] This is not the case with the narrow emission lines observed in these MOCVD-prepared QWT NWs. No such QD-like emissions are observed in GaAs/AlGaAs core−shell NWs, or in the 8 and 6 nm QWT NWs. Furthermore, the QD-like narrow emissions are observed to shift as the well width decreases to higher energy as expected from our theoretical models. We therefore believe that these QD-like localized states are related to either well-width fluctuations or alloy fluctuations near the surface of the QWT as has been observed previously in spatially resolved measurements in traditional 2D GaAs/AlGaAs QWs.[29,30] We do not, at this point, know whether the QD-like emissions are related to fluctuations along the axis of the NW or azimuthally around the NW.

Quantum Dot Temperature Dependence in 2 nm QWT. To understand the evolution of these QD-like states in the 2 nm QWT, PL images at 10 and 50 K are taken under the same excitation conditions, but using the 600 mm focal length spectrograph stage of a DILOR triple spectrometer in order to obtain higher spectral resolution (∼200 μeV) to resolve the emission widths of the narrow emission lines.

In the 10 K PL map displayed in Figure 5a, we observe intense emissions from a number of localized states on the high energy side of the PL response. Only a few of these states persist to higher temperatures, and these experience significant thermal broadening of their line widths (Figure 5c). The lower energy narrow emissions persist to higher temperatures, but the QD-like emissions disappear around 80 K in all QWT NWs indicating that the localization energies are of order 10 meV. The fact that the 2 nm QWT QD-like emissions are only bound by 10 meV provides some insight into why they are not seen in wider wells. As shown in Figure 3, the total exciton confinement energy decreases from 250 meV for the 2 nm QWT to ∼50 meV for the 8 nm QWT. Because the sensitivity of the well-width or alloy fluctuations scales directly with the confinement energy, such localizations must decrease by a *minimum* of a factor of 5 in the 8 nm well, and likely higher. That such fluctuations must be substantially less than 2 meV in the 8 nm QWT is consistent with the fact that the emission intensity is nearly continuous along the length of the NW (see Supporting Information).

A series of PL spectra of localized states centered at 1.8625 and 1.865 eV (positioned at 3 μm along the NW) as a function of temperature from 10 to 80 K are shown in Figure 5c. The line widths substantially broaden and, as expected, their positions redshift as the temperature increases. The emissions of these QD-like states also are seen to strongly quench at higher temperatures. The emission fwhm of six specific localized states (identified by yellow-dashed circles shown in Figure, 5a) with fwhm no larger than 600 μeV at 10 K are shown as a function of temperature in Figure 5d. The minimum fwhm observed in this 2 nm QWT is ∼310 μeV, which is substantially larger than the narrowest line widths observed in 2D QWs (∼5×) or in self-assembled QDs (∼155×).[29−32] The low-temperature line width of 310 μeV is equivalent to a dephasing time of only 10 ps, which likely indicates that these QD-like states are not homogeneously broadened through phonon scattering, but rather are likely closely coupled to nearby electronic states.

The temperature dependence of the QWT line widths exhibits a variety of behaviors. Several of the line widths increase almost linearly at low temperatures, but several exhibit a markedly rapid increase up to 3 meV at higher temperatures before quenching at 40 or 50 K. One QD-like peak which persists to 80 K shows a line width which increases quadratically with temperature before quenching above 80 K. The associated dephasing times for all QDs are given by the inverse of the fwhm, range from 1 to 10 ps as shown by the right axis in Figure 5d. The emission line widths of all of these QD-like states are smaller than the thermal energy k_BT, corresponding to a characteristic of QD-like PL emission. Ultralong dephasing times in self-assembled QD or QW systems have been reported with line widths (sub-μeV range) which may increase either linearly or nonlinearly as a function of temperature.[29,31] These line widths have been attributed to the interactions among the excitons and phonons, the excited states, as well as the scattering from the nearby free carriers. Sub-meV line widths (dephasing times of the order of 10 ps) at low temperatures in QDs and QWs have also been reported by several groups.[33−36] Hellmann[33] and Schultheis[34] suggest that a linear increase of line widths implies the dominant temperature-dependent dephasing mechanism is acoustic phonon scattering at temperatures less than 60 K. A nonlinear relationship between line width and temperature has also been reported by Ouerghui[35] and Gammon,[36] who suggest that optical phonons are also involved in the dephasing process in addition to acoustic phonons. The probability of subsequent excitation of the exciton to higher-lying states has also been considered in GaAs QDs by Moody et al.[37] In contrast, the QD-like states in our system are more complicated than the well-isolated QDs investigated by these researchers. In addition to the exciton−phonon interaction, the local environment, including nearby electronic states, may also be responsible for the rapid dephasing process.

The recombination lifetime of the excitons confined to these QD-like states are measured using time-correlated single photon counting. Complete time-resolved spectra are obtained by taking time decays as a function of energy from a single 2 nm QWT NW to create a time-resolved PL map as shown in Figure 6. In this map, the horizontal axis shows time after excitation by a 200 fs laser pulse, while the vertical axis shows the emission energy (Figure 6a). Several narrow emission lines are prominently observed at several different energies. The recombination lifetimes are seen to vary from dot to dot, and time decays from three QD-like states emitting at 1.812, 1.856, and 1.913 eV are seen to vary from 160 to 431 ps (Figure 6b).

DOI: 10.1021/nl5046878
Nano Lett. 2015, 15, 1876−1882

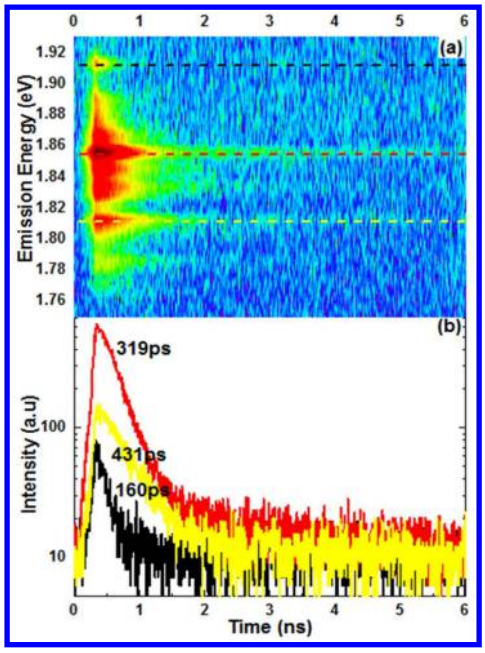

Figure 6. (a) False-colored 2D map with emission energy vs time for a single 2 nm QWT sample; darker colors represent higher intensity than lighter colors. (b) Single time decays at different emission energies.

The lifetimes of excitons confined to these QDs are less than what has been observed for excitons confined to the core of optimized GaAs/AlGaAs core-shell NWs[38,39] (~1000 ps) because of the stronger electron-hole overlap within the QWT. However, the exciton lifetimes in the QD-like states are observed to be much longer than their dephasing times, indicating that these QD-like states are strongly inhomogeneously broadened.

Conclusions. Spatially resolved PL measurements in wide QWT nanowires with well widths greater than 5 nm demonstrate that the electronic states are delocalized along the length of the NW and are consistent with theoretical calculations which show 1D-like states localized to the corners of the QWT. For QWT widths less than 5 nm, however, PL maps demonstrate that these states become spatially localized to quantum-dot-like states likely formed as a result of well-width or alloy fluctuations along the NW. This conclusion is supported by temperature-dependent measurements which show that the QWT line widths are consistent with states weakly localized by ~10 meV and coupled to nearby electronic states. This work shows a way forward in developing fabrication techniques which can optimize the smoothness of these potential fluctuations and, perhaps through modulation doping, achieve true one-dimensional conducting electronic states running along the length of the NW.

■ ASSOCIATED CONTENT

Supporting Information

Additional HR-STEM cross-sectional images and comparison of the spatially resolved PL for the 2 and 8 nm QWT NWs. This material is available free of charge via the Internet at http://pubs.acs.org.

■ AUTHOR INFORMATION

Corresponding Author

*E-mail: leigh.smith@uc.edu.

Notes

The authors declare no competing financial interest.

■ ACKNOWLEDGMENTS

We acknowledge financial support from the National Science Foundation through grants DMR-1105362, 1105121, and ECCS-1100489, and the Australian Research Council. The Australian National Fabrication Facility is acknowledged for access to the growth facilities used in this research. The FEI Titan^3 80-300 S/TEM instrument at the Monash Centre for Electron Microscopy was funded by ARC Grant LE0454166.

■ REFERENCES

(1) Saxena, D.; Mokkapati, S.; Parkinson, P.; Jiang, N.; Gao, Q.; Tan, H. H.; Jagadish, C. *Nat. Photonics* **2013**, *7*, 963−968.
(2) Wallentin, J.; Anttu, N.; Asoli, D.; Huffman, M.; Aberg, I.; Magnusson, M. H.; Siefer, G.; Fuss-Kailuweit, P.; Dimroth, F.; Witzigmann, B.; Xu, H. Q.; Samuelson, L.; Deppert, K.; Borgström, M. T. *Science* **2013**, *339*, 1057−1060.
(3) Bulgarini, G.; Reimer, M. E.; Hocevar, M.; Bakkers, E. P. A. M.; Kouwenhoven, L. P.; Zwiller, V. *Nat. Photonics* **2012**, *6*, 455−458.
(4) Reimer, M. E.; Bulgarini, G.; Akopian, N.; Hocevar, M.; Bavinck, M. B.; Verheijen, M. A.; Bakkers, E. P. A. M.; Kouwenhoven, L. P.; Zwiller, V. *Nat. Commun.* **2012**, *3*, No. 737.
(5) Wu, P. M.; Gooth, J.; Zianni, X.; Go, J.; Dick, K. A.; Thelander, C.; Nielsch, K.; Linke, H. *Nano Lett.* **2013**, *13*, 4080−4086.
(6) Tian, Y.; Sakr, M. R.; Kinder, J. M.; Liang, D.; Macdonald, M. J.; Qiu, R. L. J.; Gao, H.-J.; Gao, X. P. A. *Nano Lett.* **2012**, *12*, 6492−6497.
(7) Kempa, T. J.; Day, R. W.; Kim, S.-K.; Park, H.-G.; Lieber, C. M. *Energy Environ. Sci.* **2013**, *6*, 719−733.
(8) Kim, S.-K.; Song, K.-D.; Kempa, T. J.; Day, R. W.; Lieber, C. M.; Park, H.-G. *ACS Nano* **2014**, *8*, 3707−3714.
(9) Duan, X.; Lieber, C. M. *Nano Res.* **2015**, *8*, 1−22.
(10) Stanescu, T. D.; Tewari, S. *J. Phys.: Condens. Matter* **2013**, *25*, No. 233201.
(11) Jadczak, J.; Plochocka, P.; Mitioglu, A.; Breslavetz, I.; Royo, M.; Bertoni, A.; Goldoni, G.; Smolenski, T.; Kossacki, P.; Kretinin, A.; Shtrikman, H.; Maude, D. K. *Nano Lett.* **2014**, *14*, 2807−2814.
(12) Fickenscher, M.; Shi, T.; Jackson, H. E.; Smith, L. M.; Yarrison-Rice, J. M.; Zheng, C.; Miller, P.; Etheridge, J.; Wong, B. M.; Gao, Q.; Deshpande, S.; Tan, H. H.; Jagadish, C. *Nano Lett.* **2013**, *13*, 1016−1022.
(13) Royo, M.; Bertoni, A.; Goldoni, G. *Phys. Rev. B* **2013**, *87*, No. 115316.
(14) Ferrari, G.; Goldoni, G.; Bertoni, A.; Cuoghi, G.; Molinari, E. *Nano Lett.* **2009**, *9*, 1631−1635.
(15) Funk, S.; Royo, M.; Zardo, I.; Rudolph, D.; Morkötter, S.; Mayer, B.; Becker, J.; Bechtold, A.; Matich, S.; Döblinger, M.; Bichler, M.; Koblmüller, G.; Finley, J. J.; Bertoni, A.; Goldoni, G.; Abstreiter, G. *Nano Lett.* **2013**, *13*, 6189−6196.
(16) Heiss, M.; Fontana, Y.; Gustafsson, A.; Wüst, G.; Magen, C.; O'Regan, D. D.; Luo, J. W.; Ketterer, B.; Conesa-Boj, S.; Kuhlmann, A. V.; Houel, J.; Russo-Averchi, E.; Morante, J. R.; Cantoni, M.; Marzari, N.; Arbiol, J.; Zunger, A.; Warburton, R. J.; Fontcuberta i Morral, A. *Nat. Mater.* **2013**, *12*, 439−444.
(17) Weiß, M.; Kinzel, J. B.; Schülein, F. J. R.; Heigl, M.; Rudolph, D.; Morkötter, S.; Döblinger, M.; Bichler, M.; Abstreiter, G.; Finley, J. J.; Koblmüller, G.; Wixforth, A.; Krenner, H. J. *Nano Lett.* **2014**, *14*, 2256−2264.
(18) Arbiol, J.; de la Mata, M.; Eickhoff, M.; Morral, A. F. i. *Mater. Today* **2013**, *16*, 213−219.
(19) Joyce, H. J.; Gao, Q.; Tan, H. H.; Jagadish, C.; Kim, Y.; Zhang, X.; Guo, Y.; Zou, J. *Nano Lett.* **2007**, *7*, 921−926.
(20) Zheng, C.; Wong-Leung, J.; Gao, Q.; Tan, H. H.; Jagadish, C.; Etheridge, J. *Nano Lett.* **2013**, *13*, 3742−3748.
(21) Dwyer, C.; Maunders, C.; Zheng, C. L.; Weyland, M.; Tiemeijer, P. C.; Etheridge, J. *Appl. Phys. Lett.* **2012**, *100*, No. 191915.

DOI: 10.1021/nl5046878
Nano Lett. 2015, 15, 1876−1882

(22) Kauko, H.; Zheng, C. L.; Zhu, Y.; Glanvill, S.; Dwyer, C.; Munshi, A. M.; Fimland, B. O.; van Helvoort, A. T. J.; Etheridge, J. *Appl. Phys. Lett.* **2013**, *103*, No. 232111.
(23) Joyce, H. J.; Gao, Q.; Tan, H. H.; Jagadish, C.; Kim, Y.; Fickenscher, M. a; Perera, S.; Hoang, T. B.; Smith, L. M.; Jackson, H. E.; Yarrison-Rice, J. M.; Zhang, X.; Zou, J. *Nano Lett.* **2009**, *9*, 695−701.
(24) Perera, S.; Fickenscher, M. a.; Jackson, H. E.; Smith, L. M.; Yarrison-Rice, J. M.; Joyce, H. J.; Gao, Q.; Tan, H. H.; Jagadish, C.; Zhang, X.; Zou, J. *Appl. Phys. Lett.* **2008**, *93*, No. 053110.
(25) Spirkoska, D.; Arbiol, J.; Gustafsson, A.; Conesa-Boj, S.; Glas, F.; Zardo, I.; Heigoldt, M.; Gass, M. H.; Bleloch, A. L.; Estrade, S.; Kaniber, M.; Rossler, J.; Peiro, F.; Morante, J. R.; Abstreiter, G.; Samuelson, L.; Fontcuberta i Morral, A. *Phys. Rev. B* **2009**, *80*, No. 245325.
(26) Fickenscher, M. A.; Jackson, H. E.; Smith, L. M.; Yarrison-Rice, J. M.; Kang, J. H.; Paiman, S.; Gao, Q.; Tan, H. H.; Jagadish, C. *Appl. Phys. Lett.* **2011**, *99*, No. 263110.
(27) Hewaparakrama, K. P.; Wilson, A.; Mackowski, S.; Jackson, H. E.; Smith, L. M.; Karczewski, G.; Kossut, J. *Appl. Phys. Lett.* **2004**, *85*, 5463.
(28) Gurung, T.; Mackowski, S.; Karczewski, G.; Jackson, H. E.; Smith, L. M. *Appl. Phys. Lett.* **2008**, *93*, No. 153114.
(29) Gammon, D.; Snow, E. S.; Shanabrook, B. V.; Katzer, D. S.; Park, D. *Science* **1996**, *273*, 87−90.
(30) Gammon, D.; Snow, E. S.; Shanabrook, B. V.; Katzer, D. S.; Park, D. *Phys. Rev. Lett.* **1996**, *76*, 3005−3008.
(31) Borri, P.; Langbein, W.; Woggon, U.; Stavarache, V.; Reuter, D.; Wieck, A. *Phys. Rev. B* **2005**, *71*, No. 115328.
(32) Bayer, M.; Forchel, A. *Phys. Rev. B—Condens. Matter Mater. Phys.* **2002**, *65*, 413081−413084.
(33) Hellmann, R.; Koch, M.; Feldmann, J.; Cundiff, S.; Göbel, E.; Yakovlev, D.; Waag, A.; Landwehr, G. *Phys. Rev. B* **1993**, *48*, 2847−2850.
(34) Schultheis, L.; Honold, A.; Kuhl, J.; Köhler, K.; Tu, C. *Phys. Rev. B* **1986**, *34*, 9027−9030.
(35) Ouerghui, W.; Melliti, A.; Maaref, M. A.; Bloch, J. *Phys. E Low-Dimen. Syst. Nanostruct.* **2005**, *28*, 519−524.
(36) Gammon, D.; Rudin, S.; Reinecke, T.; Katzer, D.; Kyono, C. *Phys. Rev. B* **1995**, *51*, 16785−16789.
(37) Moody, G.; Siemens, M. E.; Bristow, A. D.; Dai, X.; Bracker, A. S.; Gammon, D.; Cundiff, S. T. *Phys. Rev. B* **2011**, *83*, No. 245316.
(38) Perera, S.; Fickenscher, M. A.; Jackson, H. E.; Smith, L. M.; Yarrison-Rice, J. M.; Joyce, H. J.; Gao, Q.; Tan, H. H.; Jagadish, C. *Appl. Phys. Lett.* **2008**, *93*, 053110.
(39) Jiang, N.; Gao, Q.; Parkinson, P.; Wong-Leung, J.; Mokkapati, S.; Breuer, S.; Tan, H. H.; Zheng, C. L.; Etheridge, J.; Jagadish, C. *Nano Lett.* **2013**, *13*, 5135−5140.

DOI: 10.1021/nl5046878
Nano Lett. 2015, 15, 1876−1882